JOURNAL OF GEOPHYSICAL RESEARCH, VOL. 107, NO. D24, 4788, doi:10.1029/2001JD001298, 2002

***Correction published 28 June 2003***

# Retrieval and characterization of ozone profiles from solar infrared spectra at the Jungfraujoch

B. Barret,[1] M. De Mazière,[1] and P. Demoulin[2]

Received 17 September 2001; revised 3 June 2002; accepted 7 June 2002; published 26 December 2002.

[1] Vertical distributions of ozone from June 1996 to November 2000 have been retrieved from high-resolution Fourier transform infrared (FTIR) solar absorption spectra recorded at the primary Network for Detection of Stratospheric Change station of the Jungfraujoch in the Swiss Alps (46.5°N, 8°E, 3580 m above sea level (asl). The retrievals were performed using the Optimal Estimation Method (OEM), both in a narrow spectral interval (1002.567–1003.2 $cm^{-1}$) and in a broad spectral interval (1000.0–1005.0 $cm^{-1}$) in the $O_3$ 9.6-μm band. A thorough characterization of the retrievals has been performed following the lines of OEM, including an information content analysis, a study of the correlations between retrieved instrumental parameters and retrieved ozone concentrations, and an evaluation of the $O_3$ profile error budget. It is demonstrated that the information content is significantly higher for spectra in the broad microwindow, resulting in higher vertical resolutions, on the order of 8 km, of the retrieved profiles extending up to 40 km, and less correlations between retrieved parameters. An independent statistical verification of the retrieval results and their characterization has been performed by comparison of the FTIR ozone profiles with independent measurements. These are the ozone profile measurements from balloon soundings at Payerne, from the microwave radiometer at Bern and the lidar at Observatoire de Haute-Provence (OHP), and the total column data from the Dobson spectrophotometer at Arosa. Applying the optimum retrieval procedure in the broad spectral interval, an excellent agreement has been found between the FTIR $O_3$ profile data and the correlative data. The largest offset of the FTIR data in comparison with the correlative data is found with respect to the lidar data in the 24- to 40-km layer, and is on the order of 5%. No systematic biases have been found in the troposphere, neither in the upper troposphere-lower stratosphere (UTLS) up to 18 km. The dispersion of the relative differences between the data sets, if any, is never larger than half of the natural ozone variability. *INDEX TERMS:* 0340 Atmospheric Composition and Structure: Middle atmosphere—composition and chemistry; 0365 Atmospheric Composition and Structure: Troposphere—composition and chemistry; 3360 Meteorology and Atmospheric Dynamics: Remote sensing; *KEYWORDS:* FTIR, ozone, profile inversion, error budget, validation

**Citation:** Barret, B., M. De Mazière, and P. Demoulin, Retrieval and characterization of ozone profiles from solar infrared spectra at the Jungfraujoch, *J. Geophys. Res.*, *107*(D24), 4788, doi:10.1029/2001JD001298, 2002.

## 1. Introduction

[2] Depending on the altitude range, the ozone vertical distribution is controlled by many different chemical and dynamical processes. Tropospheric ozone is controlled by both photochemistry and stratosphere-troposphere exchanges (STE) and the spring tropospheric ozone maximum at Northern midlatitudes remains an ''intriguing problem'' [*Monks*, 2000]. In the upper stratosphere ozone is in photochemical equilibrium while transport is controlling ozone below 30 km [*Danielsen*, 1985]. This is consistent with observations of the ozone vertical distribution at midlatitudes showing an ozone annual maximum occurring in summer at levels higher than 25 km and in early spring at levels below 25 km [*Guirlet et al.*, 2000].

[3] Many instrumental techniques are measuring ozone with a wide variety of performances. While ozone sondes are able to measure the ozone vertical profile with a very high vertical resolution, on the order of 0.1 km, from the ground up to 30 km, ground-based lidars have high vertical resolution and precision between 15 and 40 km (on the order of 2 km and 2%, respectively), and microwave spectrometers are measuring ozone profiles with a coarser vertical resolution on the order of 10 km, between 15 and 70 km. Dobson spectrophotometers are measuring total ozone columns with high precision and accuracy, on the order of 1%. Total column amounts of ozone have been retrieved from high resolution infrared solar absorption spectra recorded

[1]Institut d'Aéronomie Spatiale de Belgique, Brussels, Belgium.
[2]Institut d'Astrophysique et de Géophysique, Université de Liège, Liège, Belgium.


0148-0227/02/2001JD001298

with Fourier Transform Spectrometers (FTS) at the Jungfraujoch (46.5°N, 8°E, 3580 m above sea level (asl) [*De Mazière et al.*, 1999]. The algorithms were based on a nonlinear least squares fitting procedure in which one scaling factor applied to the whole a priori profile is adjusted until the best agreement is found between the measured and the calculated spectra. Since 1995, retrieval of profiles from Fourier transform infrared (FTIR) solar occultation spectra has become feasible using new algorithms based on the Optimal Estimation Method (OEM) developed by *Rodgers* [1976]. This retrieval method was commonly used in the microwave spectral domain. In both the microwave and the infrared spectral domains, profile retrievals are possible because of the altitude dependence of the absorption lineshapes, resulting from pressure broadening and temperature sensitivity. Therefore, the physical upper limit for height information is determined by the Doppler width of the absorption lines, which is almost altitude independent. This width being inversely proportional to the wavelength, profiles can be retrieved from microwave spectra up to 70 km altitude while in the infrared, profiles are limited to below 35–40 km.

[4] *Pougatchev* [1995] applied the OEM technique to retrieve ozone profiles from FTIR spectra recorded at Kitt Peak and at Lauder, New Zealand [*Pougatchev*, 1996]. He used a narrow spectral interval (1002.567–1003.2 $cm^{-1}$) in the 9.6-$\mu$m ozone absorption band. This choice is motivated by the presence of a wide variety of ozone absorption lines and by the absence of interfering gases. The $O_3$ absorption lines have different intensities and temperature dependences, making the retrieval sensitive from the ground up to the middle stratosphere.

[5] In this paper, we will discuss improved procedures to retrieve ozone profiles from FTIR spectra recorded at the Jungfraujoch observatory (ISSJ) between June 1996 and November 2000.

[6] The first part of the paper will be dedicated to the characterization of the retrievals. It will be demonstrated that an extension of the microwindow in comparison with the microwindow used by *Pougatchev et al.* [1995, 1996] significantly improves the retrieval results, especially in the troposphere and the upper troposphere-lower stratosphere (UTLS). The characterization includes an information content analysis and an error analysis taking into account the main sources of uncertainties.

[7] In the second part, the retrieval results will be presented and discussed, focusing on comparisons with correlative data from other instruments. The Jungfraujoch FTIR time series has a very high temporal coverage: for this study, 769 spectra recorded at solar zenith angles smaller than 75° have been selected, covering 385 days in the investigated period of four and a half years. This high coverage has allowed us to make statistically relevant comparisons for all altitude ranges with data from other ozone sensors in the same geographical area. The ozone soundings of Payerne (46.8°N, 6.95°E) were used for comparisons in the troposphere and in the lower stratosphere, while profiles from the microwave radiometer of Bern (46.95°N, 7.45°E) and the lidar from Observatoire de Haute Provence (OHP, 44°N, 6°E) were used in the stratosphere. The total columns were compared to the Dobson spectrophotometer data of Arosa (46.77°N, 9.7°E, 1820 m asl). These comparisons have proven that the FTIR data, in spite of their rather coarse height-resolution, provide reliable height-resolved information about the ozone vertical distribution.

## 2. Ozone Vertical Profile Retrieval

### 2.1. Forward Model

[8] The atmospheric transmittance spectra are simulated using a multilayer, multispecies line-by-line forward model [*Rinsland et al.*, 1982, 1984]. For each layer and each absorption line, the monochromatic transmittance is calculated on a fixed spectral grid spacing of 0.0004 $cm^{-1}$ assuming a Voigt line shape function [*Drayson*, 1976]. Density-weighted pressures, temperatures, and air masses are computed for each of the 29 layers of the model by the refractive ray-tracing subroutines FSCATM from *Gallery et al.* [1983]. In the case of the ISSJ, the lower boundary of the model is fixed at 3.58 km and the first layer extends up to 6 km. From 6 km up to 50 km, all layers are defined with the same thickness of 2 km. The layer thickness is set to 5 km between 50 and 70 km, and finally to 10 and 20 km up to the upper boundary at 100 km. The interferogram is obtained by application of a fast Fourier transform on the transmittance spectrum and the FTS Instrumental Line Shape (ILS) function is then applied to the interferogram. The ILS function takes into account a possible apodization function, the effect of the finite maximum Optical Path Difference (OPD) and the effect of the finite extension of the field of view. The forward model includes a number of additional instrumental parameters, namely a wave number shift between the measured and the simulated spectrum, the slope of the background level and the offset of the zero transmission level. The latter parameters are defined in equation (1), in which $T$ is the transmittance at wave number $\nu$, calculated for a theoretical case with zero transmission offset and constant background level equal to 1, and $T'$ is the corresponding transmittance at wave number $\nu$, simulated in case the spectrum has a zero offset $Z$ and a background level that varies linearly with wave number with slope $B$. $\nu_0$ is the lowest wave number of the selected microwindow.

$$T'(\nu) = [1 + B^*(\nu - \nu_0)]^* \frac{T(\nu) + Z}{1 + Z} \quad (1)$$

The forward model also includes a simple parameterization of symmetrical distortions of the ILS as a straight-line apodization function [*Park*, 1983] or as a parabolic function. In the first case, the value of the straight-line apodization function at maximum path difference is called the effective apodization parameter (EAP).

[9] The spectroscopic line parameters were taken from the HITRAN 1996 database [*Rothman et al.*, 1998]. Daily pressure and temperature vertical profiles were taken from the National Center for Environment Prediction (NCEP) for the actual dates and location of the measurements.

### 2.2. Retrieval Algorithm

[10] The vertical profiles of ozone were retrieved from the solar IR spectra with the SFIT2 algorithm developed at NASA Langley Research Center and the National Institute for Water and Atmospheric Research (New Zealand) and

described in previous papers [*Pougatchev et al.*, 1995; *Rinsland et al.*, 1998]. The retrieval is based on a semi-empirical implementation of the OEM [*Rodgers*, 1976, 2000]. Synthetic IR solar spectra are computed using the forward model described above. The molecular vertical profiles are iteratively adjusted according to the OEM until the residuals between the synthetic and the measured spectra get as close as possible to the noise level. Because the problem is ill-posed, the retrieval method needs a priori values of the retrieved parameters, therefore in particular a priori profiles of the target gases. The result of the retrieval is a weighted mean of the a priori information and the measurement. The weights are given by the covariance matrices of the a priori information and of the measurement, which are supposed to be representative for their respective uncertainties. The implementation of the OEM in SFIT2 is semiempirical because these covariance matrices are chosen so that the best possible fit is obtained without undesired oscillations in the retrieved profiles. The SFIT2 algorithm allows the retrieval of profiles of one or two molecular constituents together with total columns of interfering species by fitting one or more microwindows simultaneously. At the same time, some of the instrumental parameters included in the forward model may be retrieved.

### 2.3. Retrieval Parameters

[11] Based on the previous work of *Pougatchev* [1995, 1996], we used microwindows in the 10-μm region. The spectral interval between 1000 and 1005 $cm^{-1}$ has many advantages. Except for some weak absorptions of water vapour, it is free of absorptions of interfering gases. Furthermore, in this interval, ozone has hundreds of absorption lines above the noise level with very different intensities and lower state energies ($E''$). This makes the retrieval sensitive in both the troposphere and the stratosphere. The retrievals were performed using two different microwindows, namely the same one as used by Pougatchev, 1002.567–1003.2 $cm^{-1}$ and a broader one, from 1000 to 1005 $cm^{-1}$.

[12] Besides the ozone profile, we retrieved the total columns of the isotopes $^{16}O^{16}O^{18}O$ and $^{16}O^{18}O^{16}O$ in both microwindows plus the total column of water vapour in the broad microwindow. The ozone volume mixing ratios (vmr) were retrieved in the same layers as those used by the forward model. In all cases, we also retrieved the zero transmission level and the wave number shift. We used a straight line apodization to model the ILS. A first retrieval was made supposing an ideal ILS, i.e., with the EAP fixed at 1, whereas in a second retrieval exercise the latter parameter was retrieved.

[13] The ozone a priori profiles are taken from a local climatology consisting of monthly mean profiles calculated from all coincident ozone soundings at Payerne and microwave profiles at Bern, between 1995 and 1999. Data from ozone soundings were used for the profile above 3.58 km up to 23 km, the microwave data complete the profile up to 70 km and the US76 standard atmosphere above.

[14] The a priori covariance matrix was chosen diagonal with values corresponding to 25% ozone variability up to 16 km and to 20% higher up, representing the higher natural variability of ozone in the troposphere and UTLS regions. The measurement covariance matrix was also chosen diagonal with all values identical. The diagonal values represent the inverse square of the signal-to-noise ratio, for which it turned out that the best choice was 150.

## 3. Characterization of the Retrieval

### 3.1. Averaging Kernels and Information Content

[15] The OEM permits the characterization of the retrieved profiles, as described by *Rodgers* [1990, 2000]. We will first discuss the meaning and use of the so-called averaging kernels. We call "state vector" the vector x containing all the unknown parameters that will be estimated from the measurements by the retrieval. These parameters may be molecular profiles describing the state of the atmosphere as well as instrument related parameters. The retrieved state vector $x'$ is related to the true state vector x and the a priori state vector $x_a$ by

$$x' = x_a + A(x - x_a) + (\text{error terms}) \tag{2}$$

in which A is the matrix whose rows are called the averaging kernels. Equation (2) shows that each retrieved parameter is a weighted mean of all true state vector parameters with weights given by the averaging kernel. In the ideal case, the averaging kernel matrix is the unit matrix I. If we consider the subspace concerning one atmospheric molecular profile, the corresponding state vector has 29 elements each of which represents the vmr of the target molecule in one of the atmospheric model layers. In this subspace, the averaging kernels are bell-shaped functions. Their amplitudes give an indication of the sensitivity of the retrieval in each layer, and their widths of the vertical resolution for that layer.

[16] A comparison between the averaging kernels of the broad and the narrow microwindows demonstrates one of the advantages of using the broad microwindow. The ozone concentration profile averaging kernels displayed in Figure 1 show that the retrieval in the broad microwindow is more sensitive to the ozone concentrations in all layers, especially in the troposphere, with larger amplitudes of the peaks and smaller widths indicating a higher vertical resolution.

[17] A precise evaluation of the information content of the measurements has been made using the method described by *Rodgers* [2000]. According to this method, the trace of the averaging kernels matrix is the so-called number of "degrees of freedom for signal" and provides an estimate of the number of independent pieces of information contained in the measurement. Based hereupon, we estimate that the number of independent pieces of information is 4.7 in the case of the broad microwindow and only 3.0 in the case of the narrow microwindow. To quantify these independent components, we performed an eigenvector expansion of the A matrix [*Rodgers*, 1990, 2000]. If R is the matrix of right eigenvectors of A, L the matrix of left eigenvectors and Λ the diagonal matrix with the eigenvalues of A on its diagonal, one has the following relationships:

$$A = R\Lambda L^T \qquad AR = R\Lambda \qquad L^T A = \Lambda L^T$$
$$\text{and} \qquad L^T = R^{-1} \tag{3}$$

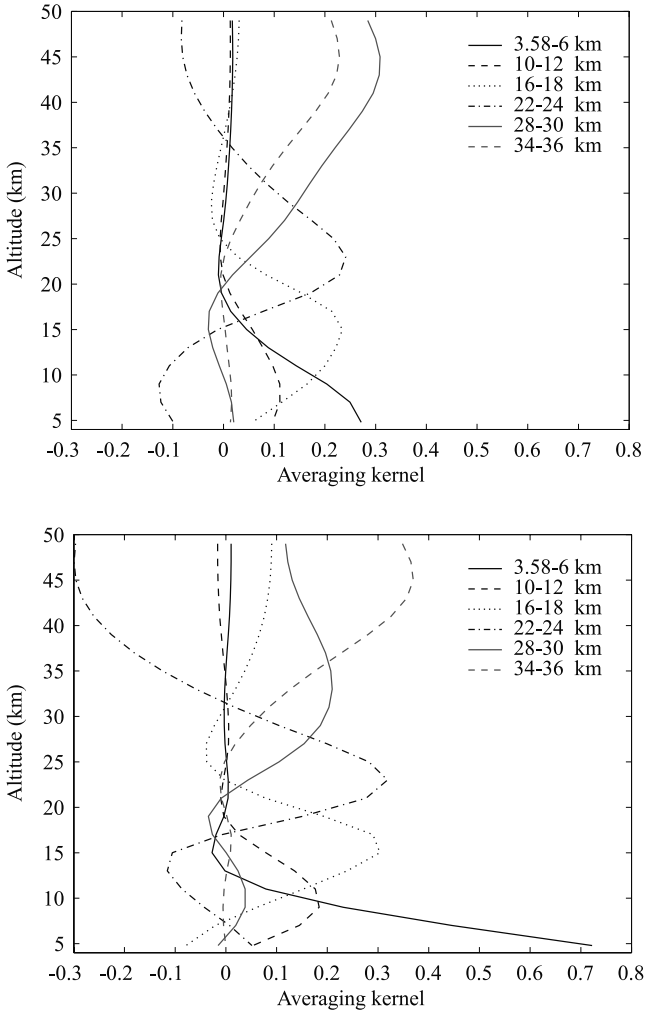


**Figure 1.** Averaging kernels for ozone profile retrievals, (i) in the narrow microwindow 1002.567–1003.2 $cm^{-1}$ (upper plot), and (ii) in the broad microwindow 1000–1005 $cm^{-1}$ (lower plot).

After multiplication of equation (2) by $L^T$ on the left, and neglecting the error terms, one obtains:

$$z' = \Lambda z + (I - \Lambda)z_a \tag{4}$$

with $z' = L^T x'$, $z = L^T x$ and $z_a = L^T x_a$ the projections of the state vectors on the right eigenvectors of A.

[18] The matrix $\Lambda$ being diagonal, equation (4) shows that components, or right eigenvectors of A, for which the corresponding eigenvalues are close to unity will be well reproduced by the measurement system, while for components with eigenvalues close to null, the retrieval will mainly reproduce the a priori state.

[19] Figure 2 shows the six leading right eigenvectors of the A matrix for the $O_3$ part of the state vector for both the broad and the narrow microwindows, together with the corresponding eigenvalues. In the narrow microwindow case, the true state contributes more than 50% to the retrieved state, only for the first three components, while in the broad microwindow case, five components have eigenvalues higher than 0.5. As for both microwindows, the shapes of the eigenvectors are quite similar, allowing conclusions to be drawn about differences in height sensitivities between both microwindows. The three leading eigenvectors whose eigenvalues are close to unity in both retrieval cases have their main peaks above 18 km. These components are therefore mainly responsible for sensitivity in the middle stratosphere, where the ozone concentration maximum lies. The fourth and fifth eigenvectors have secondary peaks between 12 km and 20 km but their eigenvalues are very different in both retrieval cases. Therefore, the retrievals in the broad microwindow with fourth and fifth eigenvalues equal to 0.93 and 0.63, respectively, are more sensitive to the $O_3$ concentration in the troposphere and in the UTLS region than the retrievals in the narrow microwindow with fourth and fifth eigenvalues equal to 0.34 and 0.08, respectively.

[20] The above information content analysis has guided us in the choice of presenting the ozone retrieval results as $O_3$ partial columns in four distinct merged layers in addition to the total column. The lowermost layer from 3.58 to 12 km covers the troposphere. The lower stratosphere from 12 to 24 km, where the vertical resolution is the highest, is cut in two 6-km layers. The last layer covers the broad altitude range 24–40 km because of a low vertical resolution. The 24-km boundary has been chosen to separate the region where ozone is controlled by photochemistry from the region where transport controls ozone. The comparison with independent measurements will confirm the conclusions drawn from the above analysis, namely that four independent components can effectively be retrieved from the broad microwindow while only three can be retrieved from the narrow microwindow which has less sensitivity in the troposphere.

### 3.2. Correlations Between Retrieved Parameters

[21] An important cause of biases in the retrieved $O_3$ profile is the existence of correlations between retrieved instrumental parameters and retrieved ozone vmr values. In order to study these correlations, we performed Monte-Carlo simulations. One thousand $O_3$ profiles were built by perturbing a standard profile with Gaussian-like functions:

$$y(z) = y_0(z)*(1 + a* \exp(-((z - b)/c))^2) \tag{5}$$

where a, the amplitude of the perturbation is a vector of 1000 random numbers that are normally distributed with a null mean and a relative standard deviation of 30%. b is the center altitude of the Gaussian perturbation: it is randomly taking a discrete value between 0 and 39 km with a 1-km step. c, proportional to the width of the Gaussian, varies randomly between 4 and 22 km with a 2-km step.

[22] These 1000 profiles were used to simulate 1000 spectra with straight-line apodization functions. The EAP was normally distributed with a mean of 1 and a relative standard deviation of 15%. The ozone profile as well as the background slope, the zero transmission level and the EAP were retrieved from these synthetic spectra. We calculated the correlation coefficients between the relative error ((retrieved-true)/true) of the retrieved instrumental parameters and the relative errors of the retrieved $O_3$ partial columns for each merged layer. The correlation coefficients for the broad and the narrow microwindow

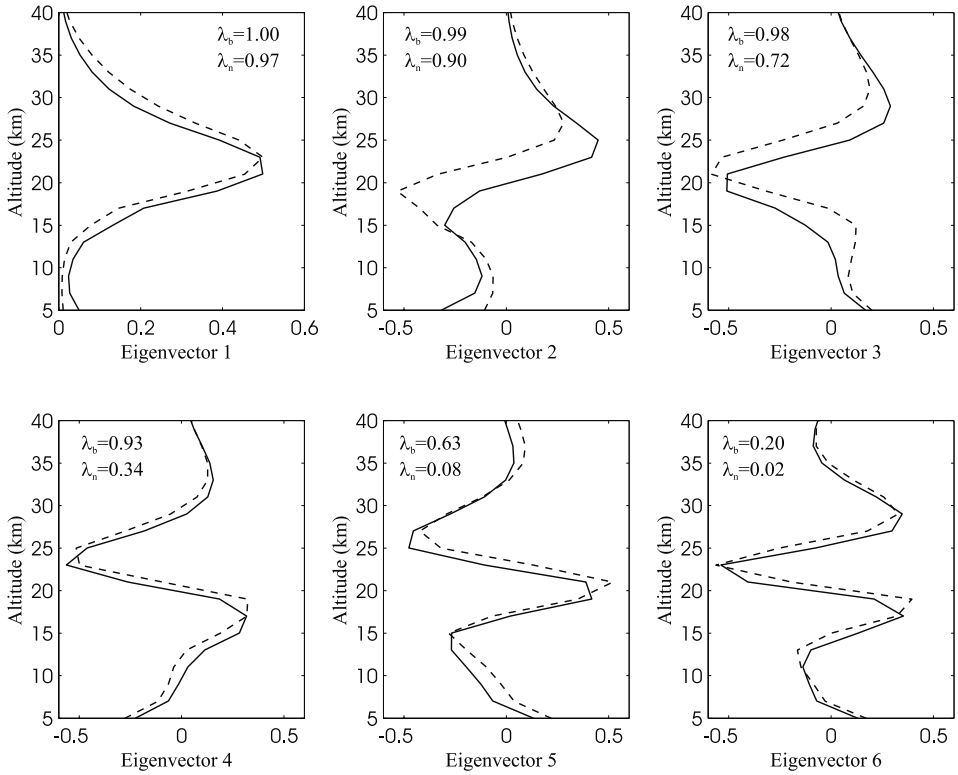


**Figure 2.** Six leading eigenvectors and their eigenvalues of the averaging kernel matrix for ozone profile retrievals, (i) in the narrow microwindow: eigenvectors in dashed lines and eigenvalues $\lambda_n$, and (ii), in the broad microwindow: eigenvectors in solid lines and eigenvalues $\lambda_b$.

are displayed in Table 1. For the narrow microwindow retrieval, the background slope is highly correlated with the two lowermost $O_3$ partial columns. The correlation is positive with the tropospheric (3.58–12 km) column, and negative with the 12- to 18-km partial column. On the contrary, the background slope is not correlated to any of the partial columns for the retrieval in the broad microwindow. Furthermore, the dispersion of the retrieved background slope is 100 times higher for the narrow microwindow retrievals. Figure 3 (upper plot) shows the clear correlation between the retrieved background slope and the retrieved tropospheric $O_3$ partial column for the narrow microwindow and the absence of correlation for the broad microwindow. The explanation of such a difference is that the tropospheric information content is more distinct in the broad microwindow than in the narrow one. This can be seen in Figure 4 in which synthetic spectra calculated for a standard atmosphere including the total atmospheric ozone profile are drawn against spectra calculated for an atmosphere containing only tropospheric ozone (3.58–12 km). From this figure, one understands that tropospheric ozone is mistaken with the background in the narrow spectral interval, because of the lack of spectral points with zero absorption on the high wave number side of the interval. Possible biases resulting from correlations between the ozone partial columns in the two lowermost layers and the slope of the background (Table 1, narrow microwindow) should be eliminated when the retrievals are performed with a constant 100% transmission level. In the absence of correlations between the slope of the background and any of the retrieved ozone partial columns (Table 1, broad microwindow), the retrieval of the slope of the background together with the ozone profile is not likely to be responsible of any biases for any of the retrieved partial columns. These observations obtained from synthetic spectra will be confirmed in section 4.2, where results from experimental spectra are discussed.

**Table 1.** Correlation Coefficients Between the Relative Errors ((Retrieved-True)/True) of the Retrieved $O_3$ Partial Columns in the Four Independent Layers Mentioned on Top and the Retrieved Instrumental Parameters (Rows), for Retrievals Performed in the Narrow Microwindow (N) and in the Broad Microwindow (B)[a]

| | 3.6–12 km | | 12–18 km | | 18–24 km | | 24–40 km | |
|---|---|---|---|---|---|---|---|---|
| Model Parameters | N | B | N | B | N | B | N | B |
| Background slope | 0.9 | 0.1 | −0.6 | 0.1 | 0.2 | 0.0 | 0.0 | 0.0 |
| Effective apodization parameter | 0.4 | 0.0 | −0.5 | 0.2 | 0.8 | −0.1 | −0.3 | 0.3 |
| Zero transmission level | 0.5 | −0.1 | −0.5 | 0.3 | 0.7 | −0.3 | −0.1 | 0.4 |

[a]The correlation coefficients are obtained through a Monte-Carlo study (see text).

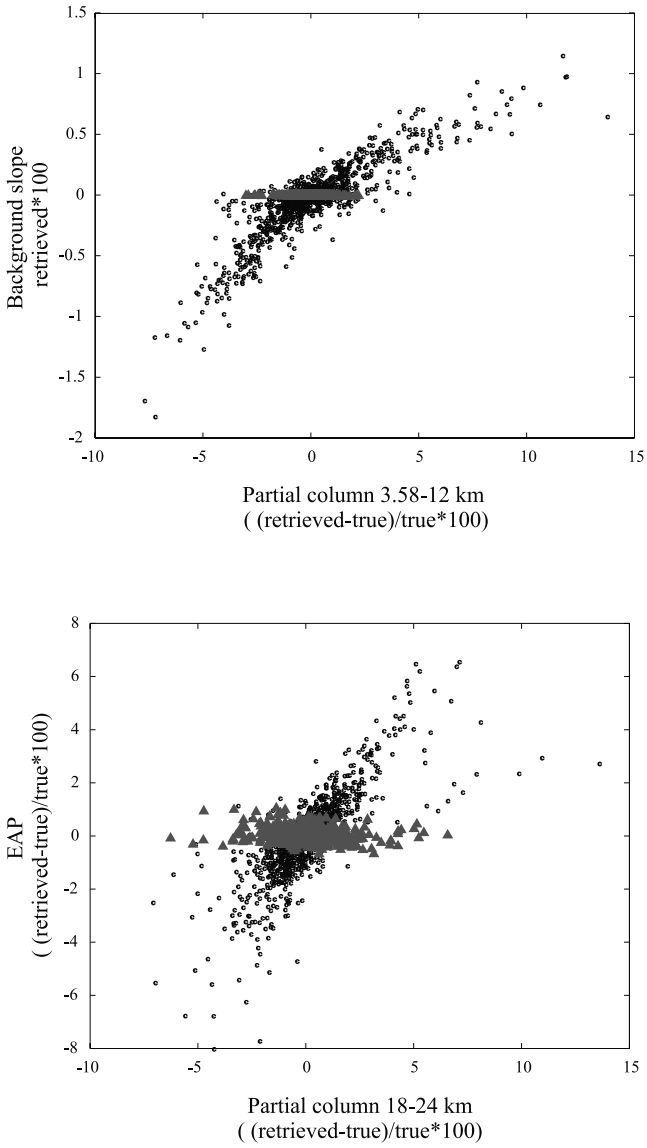


**Figure 3.** Correlation plot between (i) the retrieved background slope and the relative error of the retrieved $O_3$ tropospheric (3.58–12 km) partial column (upper plot), and (ii) the relative error of the retrieved EAP and the relative error of the retrieved $O_3$ partial column in the third layer (18–24 km) (lower plot), resulting from the Monte Carlo study (see text). Black circles: retrievals in the narrow microwindow; gray triangles: retrievals in the broad microwindow.

[23] The EAP is highly correlated with the two lowermost stratospheric partial columns (12–18 and 18–24 km) for retrievals made with the narrow microwindow. When using the broad microwindow the EAP is only slightly correlated with the uppermost partial column (24–40 km). The difference between both microwindows for the correlation between the retrieved EAP and the retrieved $O_3$ partial column in the third layer (18–24 km) is clearly shown in Figure 3 (lower plot). The correlation coefficients for the zero transmission level are similar to the ones for the EAP meaning that both parameters are mutually strongly correlated. For these two parameters, the dispersion of the retrieval error is about 10 times higher when using the narrow microwindow.

### 3.3. Error Budget

#### 3.3.1. Random Errors

##### 3.3.1.1. Smoothing Error

[24] As we have already seen (section 3.1), the OEM implies that the retrieved profile depends on the a priori one and on the averaging kernels. From equation (2) we can write the difference between the retrieved profile and the true one as

$$x' - x = (A - I)(x - x_a) \tag{6}$$

This difference is called the smoothing error and is accounting for the a priori profile contribution and for the

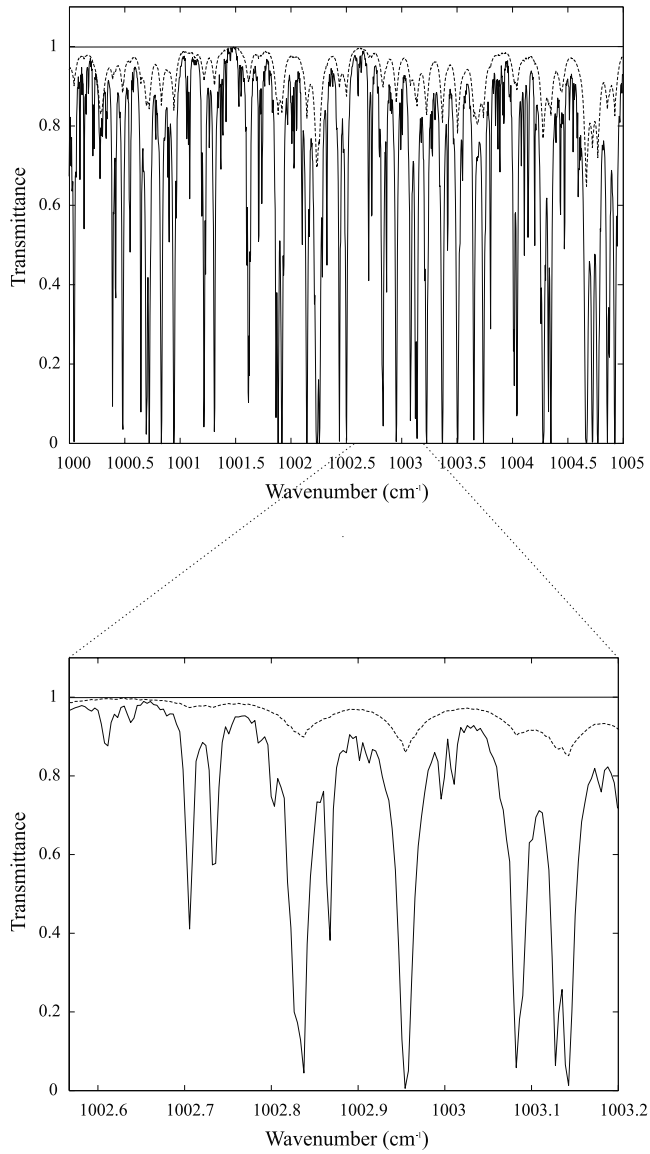


**Figure 4.** Solar absorption spectra in the 10-μm region synthesized for a standard atmosphere including the total ozone profile (solid lines), and for an atmosphere including only tropospheric ozone (3.58–12 km) (dashed lines); solar zenith angle = 60°; spectral resolution = 0.004 $cm^{-1}$. Upper plot: broad microwindow; lower plot: narrow microwindow.

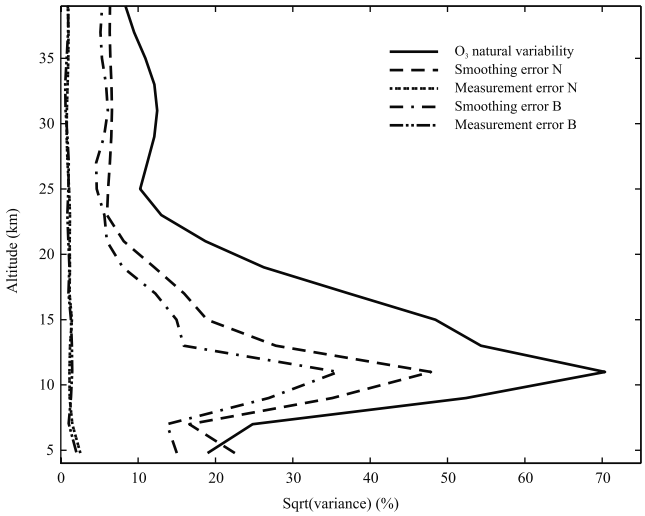


**Figure 5.** Profiles of the measurement and smoothing errors compared to the profile of ozone natural variability (N: retrievals in the narrow microwindow; B: retrievals in the broad microwindow).

smoothing of the true profile by the averaging kernels. This error can be evaluated if we have an independent estimate of the variability of the true profile and of its covariance matrix $S_x$. Then, the smoothing error covariance can be calculated as [*Rodgers*, 1990]:

$$S_s = (A - I)S_x(A - I)^T \quad (7)$$

We estimated the variance of the true ozone profile from a set of more than 700 composite ozone profiles built from ozone soundings at Payerne (up to 23 km), microwave profiles at Bern (from 23 to 70 km) and the US76 standard atmosphere ozone profile above 75 km, for 6 consecutive years (1995 to 2000). In order to account for correlations between ozone values at different altitudes, extra-diagonal terms were added to the covariance matrix $S_x$ as Gaussian functions:

$$S_{x\,ij} = \sqrt{(S_{x\,ii}\, S_{x\,jj})\exp(-((z_i - z_j)/10)^2)} \quad (8)$$

The smoothing error profiles (square root of the variances, i.e., of the diagonal values of $S_s$) calculated for both microwindows together with the ozone variability profile (square root of variances of $S_X$) are displayed in Figure 5. The smoothing error is the main source of error with a sharp maximum at 11 km where the ozone variability is also largest because of tropopause altitude variations. It is also in this altitude range that one gains most in precision by using the broad microwindow instead of the narrow one: the smoothing error is reduced by about 10% between 8 and 14 km.

**3.3.1.2. Measurement Error**

[25] Most of the ISSJ $O_3$ spectra analyzed in this work have a signal-to-noise ratio between 1000 and 4000. The "signal" is evaluated as the maximum transmittance in the considered spectral domain. The "noise" is the standard deviation of the transmittance where this transmittance theoretically should be zero, for example, beyond the optical filters spectral cut-off. The contribution of the measurement noise to the retrieval error can be estimated with the OEM [*Rodgers*, 1990]. If $S_\varepsilon$ is the covariance matrix of the noise in the measured spectra, we have:

$$S_M = D_y S_\varepsilon D_y^T \quad (9)$$

where $D_y$ is the contribution function matrix; each column of $D_y$ represents the contribution of a unit change in the corresponding element of the measured spectrum to the retrieved profile [*Rodgers*, 1990]. We use a diagonal measurement covariance matrix $S_\varepsilon$ with all values equal to $4.0\ 10^{-6}$, corresponding to a signal-to-noise ratio of 500 to calculate the measurement error. This is a conservative assumption, most of the spectra having a signal-to-noise ratio better than 1000. Measurement errors are also displayed in Figure 5. Over the whole altitude range, the measurement error is a minor contribution to the total random error with no noticeable difference between the narrow and the broad microwindow.

**3.3.1.3. Temperature Profile Uncertainties**

[26] Due to the dependence of the molecular absorption line strengths and widths on temperature, uncertainties in the temperature profile may cause errors on the retrieval results. The temperature variance profile was estimated as the profile of variance between temperatures on 5 consecutive days, averaged over 6 years. The temperature variability over 5 days is highest in the troposphere, reaching 3K at 12 km, and is around 1.5K in the stratosphere. For 12 days, one for each month of the year, spectra were synthesized using the climatological monthly mean $O_3$ profile and the actual temperature profile for that day, and retrieved with this same temperature profile to which the temperature uncertainty profile was added. The random error caused by the temperature uncertainty has been estimated as the absolute value of the mean difference between the retrieved and true profiles. For both the narrow and broad retrieval windows, the contribution of the temperature uncertainty error to the total random error is only noticeable in the uppermost layer (24–40 km).

**3.3.1.4. Water Vapour Interferences**

[27] The impact on the $O_3$ retrievals of weak absorptions of water vapour that are present in the broad microwindow has been evaluated. In order to estimate the variability of the water vapour profile in the troposphere in the region of the Jungfraujoch, we used the relative humidity profiles extracted from 462 radio soundings at Payerne between June 1996 and December 2000. The statistical analysis of these data indicates that the water vapour average vmr decreases by a factor of almost 4 from 7900 ppm in the layer between 1 and 2 km to only 2200 ppm in the layer between 3.58 and 6 km, and that its standard deviation decreases by a factor of more than 2 from 3200 to 1400 ppm. This result clearly demonstrates the advantage of the station's high altitude location regarding a possible impact of the water vapour. The uncertainties caused by the tropospheric water vapour variability have been addressed in the same way as the ones caused by the temperature uncertainty. Twelve spectra have been synthesized using the climatological monthly mean $O_3$ profiles and the average

water vapour profiles to which one standard deviation was added, and the retrievals have been performed using the average water vapour profile as the a priori and the water vapour total column as a retrieved parameter. This test has proven that the contribution of the water vapour variability to the random error of the $O_3$ retrieval is negligible (<0.1%) in all layers.

**3.3.1.5. Summary**

[28] Table 2 summarizes the nonnegligible contributions to the random error budget for the $O_3$ total column and partial columns in the four independent atmospheric layers selected for the characterization of the $O_3$ retrieval. Upon switching from the narrow to the broad retrieval microwindow, the total random error decreases significantly in all three layers below 24 km. This decrease originates mainly in the reduction of the smoothing error in these layers. For the $O_3$ partial column in the uppermost layer from 24 to 40 km and for the $O_3$ total column, the total random errors are comparable for both narrow and broad retrieval microwindows.

**3.3.2. Systematic Errors**

**3.3.2.1. Spectroscopic Parameters**

[29] The uncertainties in the spectroscopic parameters are responsible for systematic errors in the retrieved $O_3$ profiles. In the next two paragraphs, we study the impact of errors in the line intensities and in the air-broadening coefficients for the main ozone isotope, while the impacts of errors in the spectroscopic parameters of water vapour are studied in the third paragraph.

[30] $O_3$ *line intensities*: In the spectral region considered here, no error ranges are reported for $O_3$ line intensities in HITRAN 96. Our estimation of the impact of line intensities errors has been based on new measurements made by different teams. In *Smith et al.* [2001] measurements of absolute intensities of $^{16}O_3$ lines in the 9- to 11-μm regions have been performed. In the $\nu_3$ and $\nu_1$ bands, the average uncertainties over the measured lines are 2.7% and 4.4%, respectively, and the average differences with the line intensities reported in HITRAN 96 are +0.9% and −0.2%, respectively. The agreement between the measurements by *Smith et al.* [2001] and HITRAN 96 is therefore excellent. Other recent measurements of $O_3$ lines in the 10-μm regions [*De Backer-Barilly and Barbe*, 2001; *Claveau et al.*, 2001] have been used to generate a database referred to as the MIPAS Database (MD) (J.-M. Flaud et al., MIPAS database, personal communication, 2001). Compared to HITRAN 96, the $O_3$ lines of this database have values lower by (4.4 ± 3.5)% for the $\nu_1$ band and by (3.5 ± 1.4)% for the $\nu_3$ band. The MD has been used to study the systematic errors caused by line intensity uncertainties as follows. For 12 days, one per month of the year, synthetic spectra have been computed with the line intensities from the MD for all the $O_3$ lines with intensities higher than 2.0 $10^{-23}$ $cm^{-1}$/(molecule* $cm^{-2}$). Lines with intensities below this cut-off represent only 1% of the total integrated intensity between 1000 and 1005 $cm^{-1}$. These synthetic spectra have been retrieved in the broad and the narrow microwindow using the corresponding HITRAN 96 $O_3$ line intensities. The systematic error for each layer is evaluated as the mean relative difference between the retrieved and the true values. The results are similar for both microwindows and are summarized in Table 3. As could be expected from the 3.5% bias between HITRAN 96 and MD for the $\nu_3$ band (the most important one with 82% of the integrated intensity), the integrated effect is that the retrieved total column is ∼3.5% lower than the true one. But the differences between the true profile and the retrieved ones are not homogeneous in altitude. While for the three lowermost layers, the bias between the retrieved and the true partial columns is comprised between 2.0% and 3.4%, it reaches 5.6% in the 24- to 40-km layer. This altitude dependence is probably due to the fact that the relative intensity differences in the $\nu_3$ band between the MD and HITRAN 96 are linearly correlated with the logarithm of the intensity. For the strongest lines providing more sensitivity to the troposphere and to the lower stratosphere, the relative differences are less than 3% while they are more than 5% for the weakest lines which provide a larger sensitivity to the middle and upper stratosphere.

[31] $O_3$ *air-broadening coefficients*: In HITRAN 96, the air-broadening coefficients are given with an error range of 5% to 10%. The same procedure as used for the $H_2O$ vapour interferences has been used for estimating the impact of the uncertainties in the air-broadening coefficients. The synthetic spectra have been computed with the air-broadening coefficients of all the $O_3$ lines multiplied by 1.05 and have been retrieved in the broad and the narrow microwindow using unperturbed coefficients. The air-broadening coefficient uncertainties affect the retrieval to less than ±5% in all layers and have almost no influence on the retrieval of the total columns. One does not observe any significant differences between the results from both microwindows (Table 3).

[32] $H_2O$ *spectroscopic parameters*: In the MD (J. M. Flaud et al., personal communication, 2001), new water vapour spectroscopic parameters replace the HITRAN 96 parameters. The five strongest water vapour lines present between 1000 and 1005 $cm^{-1}$ have intensities up to ∼43% lower in MD than in HITRAN 96 while the air-broadening coefficients are up to ∼46% higher. The impact of these differences has been estimated as above for the $O_3$ line intensities. The synthetic spectra were simulated using the MD $H_2O$ spectroscopic parameters while they were retrieved with the HITRAN 96 spectroscopic parameters. For all the layers the difference between the retrieved and the true partial columns are negligible (<0.3%). Nevertheless, the use of these new parameters improves the quality of the fit of experimental spectra and MD appears to be the best choice for future FTIR data.

**3.3.2.2. Effective Apodization**

[33] The effect of systematic distortions of the instrumental line shape can be evaluated for retrievals performed with a fixed EAP. The same procedure as the one used for the estimation of the sensitivity to the air-broadening coefficient uncertainties was used with spectra synthesized with an EAP of 0.9 and retrieved with a fixed EAP of 1.0. The results displayed in Table 3 show that except in the 24- to 40-km layer for which the error is 3% higher in the case of retrievals performed in the broad microwindow, the sensitivity of the retrieval to line shape distortions is almost identical for both microwindows. It is particularly important in the two uppermost layers (18–24 and 24–40 km) with errors between 5% and 8%. The expected decrease of the error caused by ILS distortions when the

EAP and the ozone profile are retrieved simultaneously is confirmed in section 4.1.

## 4. Retrieval Results for Ozone at the Jungfraujoch

[34] In this study, we analyzed all the ISSJ spectra in the 1000–1005 $cm^{-1}$ spectral range recorded at solar zenithal angles smaller than 75° between June 1996 and November 2000. The spectra in this region were obtained with a commercial BRUKER 120 HR FTS operating with a HgCdTe detector with optical path differences (OPD) of 125 and 82 cm and aperture angles of 4.78 and 5.98 mrad, respectively. The signal-to-noise ratio in the investigated spectral domain lies between 1000 and 4000 (see section 3.3 for details); the higher signal-to-noise ratios hold for spectra recorded at smaller solar zenith angles due to longer integration times.

[35] The retrieved vertical distributions of ozone have been compared to profile data obtained with three other observation techniques. From the ground up to 30 km, the profiles were compared to the soundings from Payerne. The ozone sondes are Brewer-Mast type sondes, launched about 3 times a week. They measure the ozone profile with a vertical resolution of 200 m. From comparisons with ECC sondes, we can evaluate that their precision lies between ±5% and ±12% while their accuracy is better than ±15% [*Stübi et al.*, 1999]. From 15 km up to 40 km comparisons have been performed with the ozone profile data from the microwave radiometer at Bern and the lidar at OHP. The vertical resolution of the OHP lidar measurements is altitude dependent and ranges from 0.5 km at 20 km to 2 km at 30 km and 4 km at 40 km. Their precision decreases from ±2% below 20 km to more than ±10% at 40 km and their accuracy is estimated to be on the order of ±3% [*Guirlet*, 2000]. The microwave radiometer at Bern provides ozone profiles from 15 to 70 km with an altitude resolution of 10 to 15 km and a precision better than ±5% between 20 and 40 km [*Peter and Kämper*, 1995]. The retrieved $O_3$ total columns have been compared to total column data from the Dobson spectrophotometer at Arosa that have a precision and an accuracy on the order of ±1% [*Staehelin et al.*, 1998]. The altitude difference between Arosa (1820 m asl) and the Jungfraujoch (3580 m asl) was taken into account by subtracting the corresponding ozone amount calculated from the ozone soundings from Payerne.

[36] In a first step all the profiles have been converted to ozone integrated columns (Dobson Unit, DU) in the same layers as the ones used for the FTIR retrievals. Microwave volume mixing ratio profiles were interpolated on the FTIR layer boundaries, daily averaged (from 0800 to 1600 LT) and then converted into partial columns by multiplication with the partial columns of air calculated from the NCEP pressure/temperature data that are used for the FTIR retrievals. For the high vertical resolution ozone soundings and lidar profiles, the concentrations were integrated from the bottom to the top of each 2-km layer.

[37] When comparing profiles retrieved by two instruments one must not forget to take into account the instruments' different vertical resolutions [*Connor et al.*, 1994]. If we consider that the real state of the atmosphere is given by the profile $x_h$ measured with the best vertical resolution and that the only source of error is the smoothing error, as this is the dominant error source, the retrieval should produce a smoothed profile $x_s$ given by equation (2) with x replaced by $x_h$ and without the additional error terms:

$$x_s = x_a + A(x_h - x_a) \tag{10}$$

This equation has been applied to the ozone soundings and the lidar profiles whose vertical resolutions are higher than those of the FTIR profiles, but not to the microwave profiles, which have a comparable resolution. In equation (10), $x_h$ must cover the same altitude range as the averaging kernels. Therefore, above 30 km, the sonde profiles have been completed by the FTIR a priori profile. The same procedure has been applied below 17 and above 41 km for the lidar profiles.

[38] We have compared the FTIR profiles and the correlative profiles measured by all three other instruments on a statistical basis. The statistics for the whole investigated time period is based on 156 coincident days with FTIR measurements and ozone soundings, 329 coincident days with FTIR and microwave measurements and 133 days with FTIR and lidar measurements. The discussion of the results of these comparisons is subdivided into two parts. A first part (section 4.1) is dedicated to the study of the influence of the retrieval of the EAP on the differences between the ozone profiles retrieved from the FTIR and the correlative profiles obtained with the above mentioned techniques. The second part (section 4.2) is devoted to a general discussion of the results of the intercomparisons with the FTIR profiles obtained in the best retrieval conditions.

### 4.1. Influence of the EAP Retrieval

[39] The EAP is accounting for symmetrical distortions of the ILS of the spectrometer as well as for a smearing effect due to the sampling of changing air masses during the recording time for one spectrum [*Park*, 1982, 1983]. At the beginning of the time period under study (June 1996 to November 2000), the performance of the instrument degraded gradually until 7 June 1997, when the FTS was realigned (R. Zander, private communication, 2001). As we have seen in section 3, the retrieved EAP is far less correlated with the retrieved profile and its error dispersion is 8 times lower if the retrievals are performed in the broad microwindow. Therefore, we will now discuss in more detail the possible impacts of EAP on the retrieval in the broad microwindow. As the EAP is resolution dependent, we will select for this particular study only spectra recorded at 0.004 $cm^{-1}$ resolution (OPD = 125 cm). Figure 6 draws the relative differences between FTIR profiles and ozone sonde, lidar and microwave profiles, for four consecutive periods of 1 year, each year taken from 1 June to 31 May of the next civil year. The black lines represent retrievals in which the EAP is retrieved simultaneously with the other parameters, the gray lines represent retrievals with fixed values of the EAP (EAP = 1.0). In agreement with the predictions discussed in section 3.3.2, the EAP uncertainty has little impact below 18 km but it is the cause of a large oscillation in the profile above this altitude. This effect is clear for the first year with relative differences of FTIR ozone data with soundings and microwave data of more than 30% at 23 km and with lidar data of almost 20%

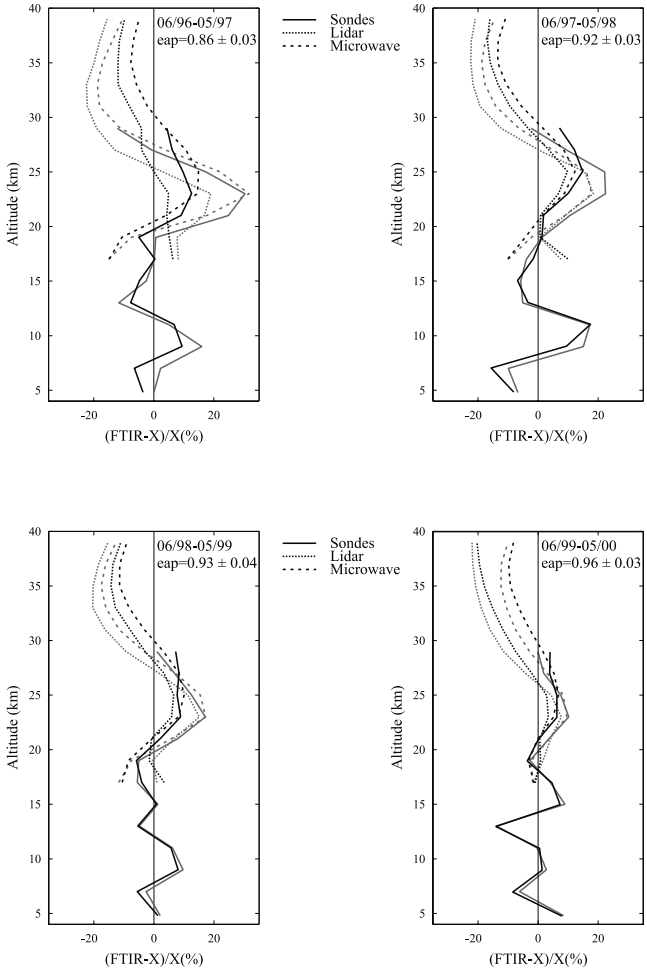


**Figure 6.** Altitude dependence of the relative difference between the $O_3$ vertical profiles from FTIR and correlative (X) data for four consecutive years between June 1996 and end of May 2000. X stands for ozone sondes (solid lines), microwave radiometer (dashed lines) and lidar (dotted lines), FTIR retrievals have been performed with retrieval of the EAP (black lines) and with a fixed EAP (EAP = 1, gray lines).

between 30 and 35 km. The FTIR profiles are getting much closer to the correlative data if the EAP is retrieved also, with differences falling below 15% at all altitudes. After the instrument realignment of June 1997, the gain in accuracy from fitting the EAP is less pronounced. But still, in all cases, the agreement with the correlative data is always better if the EAP is part of the retrieved parameters. The same conclusions can be drawn from Figure 7 summarizing these results for the merged layers. The EAP retrieval is especially critical for the third (18–24 km) and fourth layers (24–40 km) as was already predicted (Table 3). In the third layer, for retrievals with fixed EAP, the positive bias between the FTIR ozone data and all correlative data is decreasing from the first to the last year. This decrease is especially pronounced in the bias relative to the ozone soundings that is falling from 20% in 96/97 to 4% in 99/00. In comparison, when the EAP is retrieved together with the ozone profiles, this bias relative to the ozone soundings gets more stable, decreasing only slightly from 6% in 96/97 to 1% in 99/00. In the fourth layer, the biases relative to lidar and microwave data are both negative throughout the 4 years when using a fixed EAP while they become positive and less negative, respectively, when the EAP is retrieved simultaneously with the ozone profiles. The effect of the instrument misalignment in 1996–1997 is well detected by SFIT2, with a retrieved EAP of 0.86 ± 0.03 during that period. After the realignment in June 1997, the retrieved EAP is stable within the error bars, with a mean value of 0.94 ± 0.03 (]). It must be noticed that the ILS is only roughly approximated with a single EAP. Nevertheless, it is clear from our analyses, that the retrieval of this approximate parameter is improving the retrieval results and that it allows us to use the whole time series of FTIR spectra, including ILS changes, for retrieving ozone profiles in a consistent way, from the ground up to 40 km altitude.

### 4.2. General Comparison

[40] Figure 8 displays the relative differences and their relative standard deviations (RSD) between the FTIR data and all correlative data mentioned above, for both FTIR retrieval microwindows, when the EAP is retrieved in the fitting. For comparisons with sonde and lidar data the differences with profiles smoothed by the before mentioned procedure (equation (10)) are also displayed. The statistical analyses concerning the $O_3$ partial columns in the four merged layers and concerning the $O_3$ total column are gathered in Table 4. Following the discussion from section 3.2 about correlations between the slope of the background and the retrieved ozone partial columns, the results displayed are for retrievals performed with a constant 100% transmission level in case of the narrow microwindow, and with a retrieved slope of the background in case of the broad microwindow.

[41] Below 20 km, the bias between FTIR and Payerne changes significantly when retrieving $O_3$ from the narrow or from the broad microwindow. The profiles retrieved from the narrow microwindow have a negative bias in the lower troposphere compensated by a positive bias in almost all the layers up to 18 km. With the broad microwindow, the absolute biases are never larger than 10%. In terms of merged layers (Table 4), this behavior is translated into a negative bias of 4.4% in the 3.58- to 12-km layer and a positive one of 6.2% in the 12- to 18-km layer for the narrow microwindow, whereas the biases disappear for the broad microwindow.

[42] The large opposite biases obtained with the narrow microwindow are due to the lack of information about the ozone concentration in the troposphere and in the UTLS region contained in this microwindow as discussed in section 3.1. They grow even larger (−11.8% and 8.7%) if one includes the background slope in the set of retrieved parameters, thus confirming the discussion of section 3.2 regarding the possible impact of correlations between the retrieved instrumental parameters and the ozone profiles.

[43] In the middle and upper stratosphere (18 to 40 km), the profiles of relative differences are not significantly different for both microwindows. In both cases, the FTIR profiles are oscillating relative to the profiles measured by the other techniques, but apart from some exceptions above 30 km, the absolute relative differences are always lower than 10%. Anyway, these oscillations are not very signifi-

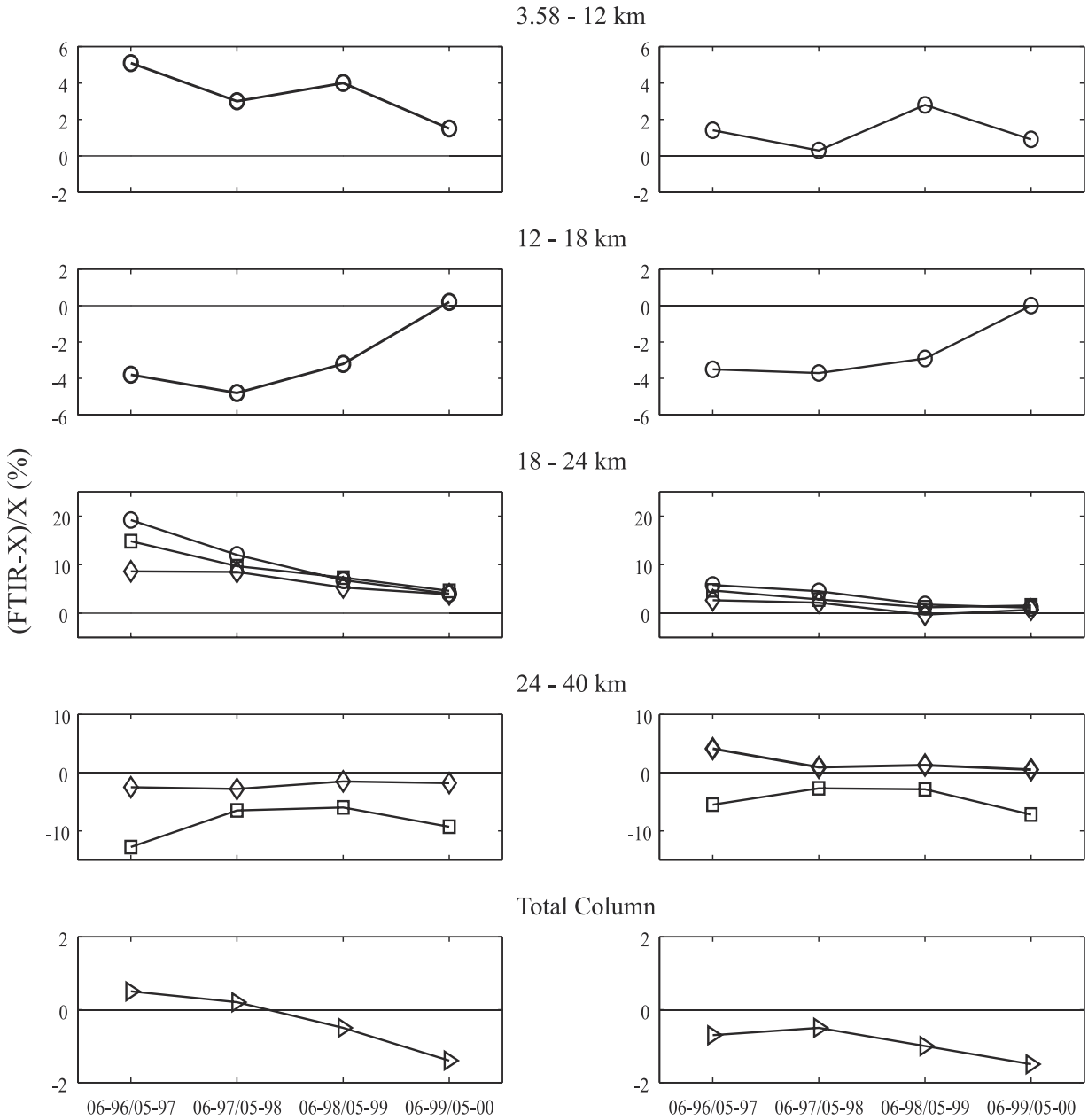


**Figure 7.** Relative differences between the partial columns and total columns retrieved from the FTIR spectra including retrieval of the EAP (right plots) and with EAP fixed to 1 (left plots) and the partial columns and total columns measured by different instruments (X). Circles: sondes; squares: lidar; diamonds: microwave radiometer; triangles: Dobson spectrophotometer.

cant, as one must consider that the real information content is limited to the merged layers, and that the agreement found here is very good. In the 18- to 24-km layer, the relative differences with the other instruments are all lower than 4.2% and hardly significant taking into account the RSD. In the 24- to 40-km layer, the agreement with both the microwave and the lidar profiles improves for the retrieval in the broad microwindow. In this layer, the relative differences with the profiles measured by the microwave spectrometer are 5% lower than with the profiles measured by the lidar.

[44] The profiles of the RSD of the differences are very similar for both microwindows and are qualitatively comparable to the random errors calculated in section 3 (Figure 5). Nevertheless, the gain in precision relative to the ozone soundings is smaller than predicted by the error analysis. While the use of the broad microwindow should have made the total random error decrease by at least 4.5% in the two lowermost layers (Table 2), we gain less than 1% in the RSD relative to the soundings (Table 4).

[45] Above 18 km, for comparisons with any of the three techniques, the RSD are identical for both retrieval microwindows and are comparable to the ones predicted. The smoothing of the sonde and lidar profiles according to equation (10) have no significant impact on the relative

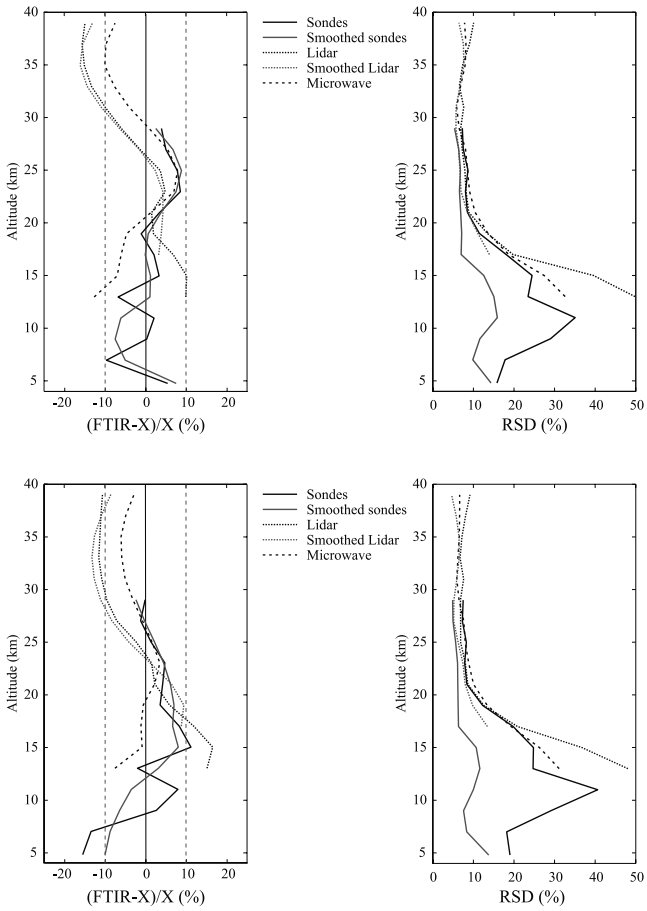


**Figure 8.** Altitude dependence of the relative differences (left plots) and relative standard deviations of the differences (RSD, right plots) between the ozone vertical profiles from FTIR and from a correlative measurement X; X stands for ozone sondes (solid lines), lidar (dotted lines) and microwave radiometer (dashed line), respectively. For the differences between smoothed and nonsmoothed: see text. The FTIR profiles result from retrievals in the broad microwindow (upper plots) and in the narrow microwindow (lower plots).

difference profiles but reduces significantly the RSD of the differences below 20 km. This is in good agreement with the error analysis performed in section 3.2 that showed that the smoothing error was the main source of random error below 20 km (Figure 5 and Table 2). For merged layers the reduction of the RSD when smoothing is applied is mainly noticeable in the tropospheric (lowermost) layer.

[46] The total columns retrieved from the FTIR spectra are in very good agreement with the total columns measured with the Dobson spectrophotometer at Arosa. With a bias of $(-0.8 \pm 2.6)\%$, our results are within the limits predicted by the error analysis (Tables 2 and 3). They agree also well with the biases between total column data retrieved from different FTIR microwindows selected in five absorption bands of $O_3$ and Dobson spectrophotometer total column measurements on the same day at Lauder ranging from $(-4 \pm 3)\%$ to $(2 \pm 3)\%$ [*Rinsland et al.*, 1996].

[47] In summary, the partial and total columns retrieved from FTIR spectra in the broad microwindow agree very well with correlative data from sonde, lidar, microwave and Dobson instruments. A significant bias was found only in the 24- to 40-km altitude range, in comparison with the lidar data but not with respect to the microwave data, and it is therefore not necessarily due to an error in the FTIR data. Regarding the $O_3$ partial columns in all the merged layers and for the total columns, the RSD of the differences between the FTIR and the correlative data are all small compared to the natural variability of ozone (Table 4).

[48] Besides the general statistics covering the whole time period, it is interesting to study how the FTIR measurements reproduce observed ozone variations. In order to quantify the seasonal variations captured by the different instruments, a single sinusoid with a period of 1 year has been fitted through the time series of ozone partial column data from each instrument, with a nonlinear least squares fitting procedure.

[49] The total columns time series measured by the FTIR spectrometer and the Dobson spectrophotometer are plotted in Figure 9. The seasonal variations reproduced by both instruments are almost identical. The phase shift of 12 days between the annual ozone maxima does not cause a measurable annual sinusoidal variation of the discrepancy (lower plot). This improves upon the findings by *De Mazière et al.* [1999], who found an offset of $-0.9\%$ and an amplitude of 2.8% for a sine fit to the differences between the Brewer data from Arosa and the FTIR total columns retrieved with a single scaling factor of the ozone a priori profile taken from a tropopause dependent seasonal climatology. The disappearance of a seasonal cycle in the discrepancy between UV and IR measurements is probably due to the use of the FTIR profile retrieval algorithm instead of the common total columns retrieval algorithm.

[50] The time series of $O_3$ partial columns are displayed in Figure 10. In order to enhance the visibility, sine fits are only displayed for the FTIR time series. Nevertheless, the sine fit parameters are in excellent agreement among all data sets from the different instruments, with a maximum phase

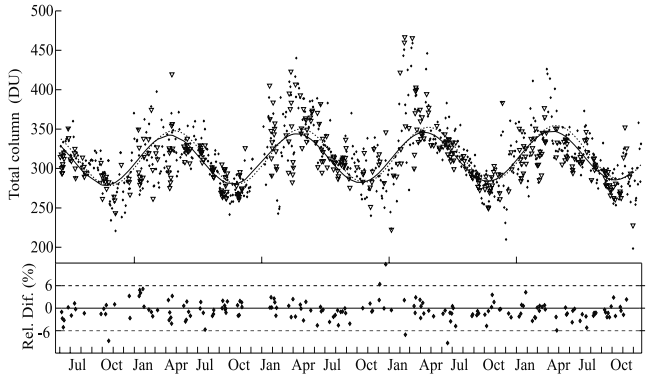


**Figure 9.** Upper plot: Ozone total columns above 3.58 km measured by the ISSJ FTIR spectrometer (empty triangles) and by the Arosa Dobson spectrophotometer (full diamonds). Corresponding annual cycles are indicated by sine fits, with solid and dashed lines for FTIR and Dobson, respectively. Lower plot: total columns relative differences for coincident days.

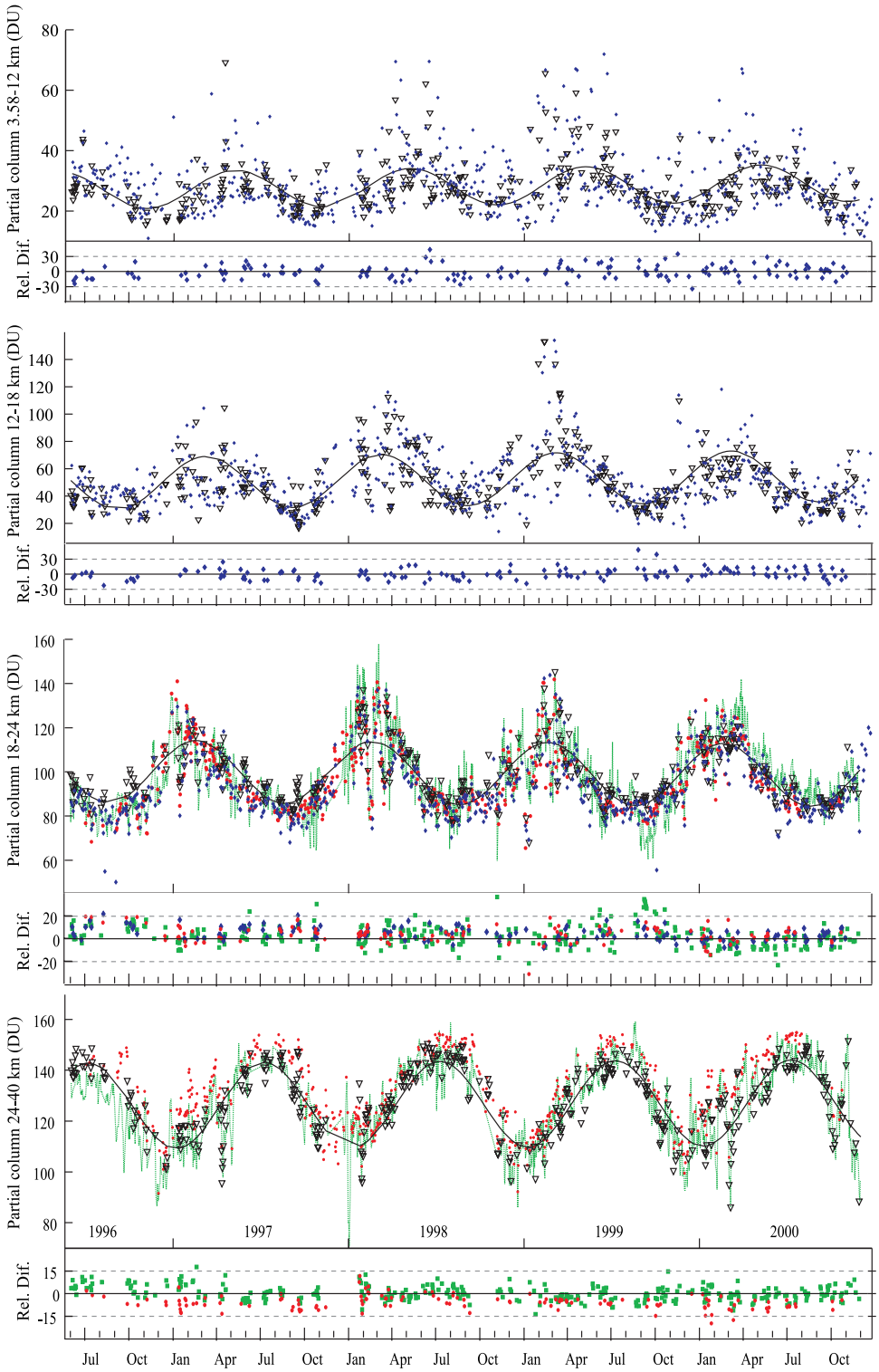


**Figure 10.** Time series of ozone partial column data for four layers 3.58–12, 12–18, 18–24, and 24–40 km (from top to bottom) as measured by different instruments: black empty triangles: FTIR; blue diamonds: sondes; green dotted lines: microwave radiometer; orange circles: lidar. The FTIR annual cycles are indicated by sine fits in black solid lines. For each layer, the relative discrepancies between the ozone data from the FTIR and the other instruments (FTIR-X)/X, in %, are shown in the lower plots.

difference of 9 days between FTIR and microwave data in the 24- to 40-km layer. The peak-to-peak amplitude of the ozone seasonal cycle is also well captured by the FTIR data in all the layers. The largest discrepancy occurs between the FTIR and the microwave data in the third layer (18–24 km) with the peak-to peak amplitude calculated from the FTIR retrievals 5.8 DU lower than the one amplitude measured by the microwave spectrometer (34.0 DU).

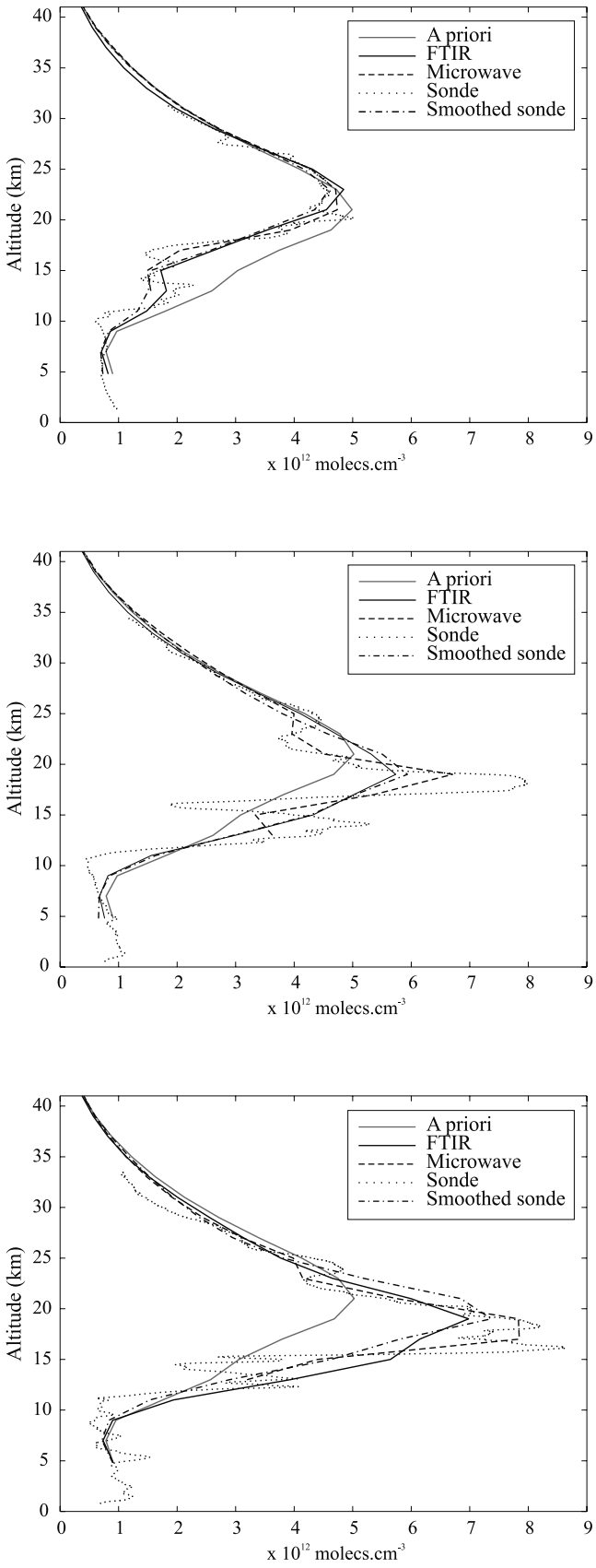


[51] During the active winter-spring periods of 1997–1998 and 1998–1999, one observes (Figure 10) very rapid variations of the ozone partial columns in the three uppermost layers, caused mostly by dynamical effects like southwards excursions of the polar vortex [*Calisesi et al.*, 2001]. Nevertheless, no sign of such high-frequency variations can be found in the plot of relative differences between the $O_3$ partial columns from the FTIR and the other instruments. This demonstrates that the FTIR instrument is able to capture the ozone variations in the selected layers independently. The correlation coefficients between the relative differences (FTIR-X)/X (with X any of the three correlative measurement techniques) for adjacent layers have been calculated. With all correlation coefficients lower than 0.1, we have a quantitative evidence of the independence between the retrieved layers.

[52] Particular $O_3$ profiles measured on 3 days in March 1999 are displayed in Figure 11 together with correlative profiles measured by the microwave radiometer at Bern and sonde profiles from Payerne. These days have been chosen during a dynamically very active period with Potential Vorticity (PV) values at 475 K above the Jungfraujoch varying from 21 PVU on 12 March to 27 and 26 PVU on 15 and 17 March. The evolution of the ozone vertical distribution is very well captured by the FTIR measurements. Comparison with the sonde profiles and with the sonde profiles smoothed by the averaging kernels of the FTIR retrieval clearly shows that most of the discrepancies between the sonde profiles and the FTIR profiles are due to the coarse vertical resolution resulting from the smoothing applied to the true profile during the retrieval.

## 5. Summary and Conclusions

[53] The results presented in this study demonstrate that the vertical distribution of ozone can be retrieved from high resolution FTIR solar spectra in four independent layers covering the altitude range from the ground up to the middle stratosphere. The procedure proposed earlier by *Pougatchev* [1995, 1996] has been modified in order to obtain the most reliable results at all atmospheric levels throughout the whole investigated time period (June 1996 to November 2000). The extension of the microwindow boundaries from 1002.56–1003.2 $cm^{-1}$ to 1000.0–1005 $cm^{-1}$ has been shown to increase the information content in the troposphere and lower stratosphere. Furthermore, it has been demonstrated that the EAP can be retrieved simultaneously with the ozone profiles in a more accurate and more independent way if one uses the broad retrieval microwindow. These conclusions have been drawn from a theoretical characterization of the retrievals, and have been confirmed by the comparisons between the time series of ozone profiles retrieved from more than 4 years of FTIR

**Figure 11.** (opposite) Individual daily ozone profiles measured by ozone sondes (dotted line), microwave radiometer (dashed line) and FTIR spectrometer (black solid line). In addition, the sonde profiles smoothed by the FTIR retrieval averaging kernels are represented by the dashed-dotted line and the FTIR a priori profile by the gray solid line. Days are: 12 March 1999 (upper plot), 15 March 1999 (middle plot), and 17 March 1999 (lower plot).

spectra recorded at the Jungfraujoch and correlative profiles measured by three other types of ozone sensors, namely ozone soundings from Payerne, lidar data from OHP and microwave radiometer data from Bern. The extension of the microwindow has lead to the disappearance of the biases of the FTIR data in the troposphere and in the UTLS relative to the ozone soundings of Payerne. Fitting the EAP simultaneously with the ozone profiles has homogenized the FTIR height-resolved ozone time series above 18 km as compared to the other three series of correlative data. The error budget derived from the theoretical error analysis has been found to agree well with the results from the statistical comparisons with the correlative data. The offsets between the FTIR height-resolved ozone data and the correlative data are always smaller than 5.5%, in any altitude layer, and the dispersion of the relative differences, if any, is never larger than half of the natural ozone variability. The amplitudes and phases of the seasonal cycles derived from FTIR measurements agree well with the ones derived from the other measurements, in all relevant layers. Short term variations of the ozone vertical distribution are also well captured by the FTIR measurements in the selected layers.

[54] This paper has therefore shown that vertical inversion of ground-based FTIR spectra is a useful tool for the derivation of partial column abundances in the free troposphere and in a limited number of atmospheric altitude ranges. The capabilities of the method have been demonstrated for ozone. Extension to other species like CO, $CH_4$ and $N_2O$ is in progress. It is clear already that the FTIR inversion results will be very useful for validating and complementing satellite tropospheric data for a number of species.

[55] **Acknowledgments.** The authors thank the OSTC Services of the Belgian Prime Minister (contracts ESAC CG/DD/O1A and research project MO/35/007) and the European Commission (contract COSE, ENV4-CT98-0750) for supporting this research. Thanks are due to P. Viatte and B. Henchoz of the Station Aérologique of the Swiss Meteorological Institute at Payerne in Switzerland for providing us with Dobson data from Arosa and ozone soundings from Payerne. N. Kämpfer and Y. Calisesi of the Institute of Applied Physics of the University of Bern, Switzerland, are acknowledged for providing us with the $O_3$ profiles data from the Ground-Based Microwave Ozone Sensor (GROMOS) in Bern. We thank S. Godin of the Service d'Aéronomie of the CNRS, France, who provided us with the lidar profiles of the Observatoire de Haute-Provence in France. B. Carli from the IROE of CNR, Italy, and J.-M. Flaud from the LPM of the CNRS, France, are acknowledged for providing us with the MIPAS database. We further thank all our colleagues of the Royal Observatory of Belgium, the University of Liège, and the Belgian Institute for Space Aeronomy who contributed to the observations at the Jungfraujoch station. The work would have been impossible without the support from the Jungfraujoch Hochalpine Forschungsstation.

## References

Calisesi, Y., H. Wernli, and N. Kämpfer, Midstratospheric ozone variability over Bern related to planetary wave activity during the winters 1994–1995 to 1998–1999, *J. Geophys. Res.*, *106*, 7903–7916, 2001.

Claveau, C., C. Camy-Peyret, A. Valentin, and J. M. Flaud, Absolute intensities of the $\nu_1$ and $\nu_3$ bands of $^{16}O_3$, *J. Mol. Spectrosc.*, *06*, 115–125, 2001.

Connor, B. J., D. E. Siskind, J. J. Tsou, A. Parrish, and E. E. Remsberg, Ground-based microwave observations of ozone in the upper stratosphere and mesosphere, *J. Geophys. Res.*, *99*, 16,757–16,770, 1994.

Danielsen, E. F., Ozone transport, in *Ozone in the Free Atmosphere*, edited by R. C. Whitten and S. S. Prasad, 123–159, Van Nostrand Reinhold, New York, 1985.

De Backer-Barilly, M.-R., and A. Barbe, Absolute intensities of the 10-μm bands of $^{16}O_3$, *J. Mol. Spectrosc.*, *205*, 43–53, 2001.

De Mazière, M., O. Hennen, M. Van Roozendael, P. Demoulin, and H. De Backer, Daily ozone profile model built on geophysical grounds, for column retrieval from atmospheric high-resolution infrared spectra, *J. Geophys. Res.*, *104*, 23,855–23,869, 1999.

Drayson, S. R., Rapid computation of the Voigt profile, *J. Quant. Spectrosc. Radiat. Transfer*, *16*, 611–614, 1976.

Gallery, W. O., F. X. Kneizys, and S. A. Clough, Air mass computer program for atmospheric transmittance/radiance calculation: FSCATM, *Environ. Res. Rep. 828, Rep. AFGL-TR-83-0065*, 145 pp., Air Force Geophys. Lab., Bedford, Mass., 1983.

Guirlet, M., P. Keckhut, S. Godin, and G. Mégie, Description of the long-term ozone data series obtained from different instrumental techniques at a single location: The Observatoire de Haute Provence (43.9°N, 5.7°E), *Ann. Geophys.*, *18*, 1325–1339, 2000.

Monks, P. S., A review of the observations and origins of the spring ozone maximum, *Atmos. Environ.*, *34*, 3545–3561, 2000.

Park, J. H., Effect of interferogram smearing on atmospheric limb sounding by Fourier transform spectroscopy, *Appl. Opt.*, *21*, 1356–1366, 1982.

Park, J. H., Analysis method for Fourier transform spectroscopy, *Appl. Opt.*, *22*, 835–849, 1983.

Peter, R., and N. Kämpfer, Short-term variations of midlatitude ozone profiles during the winter 1994–1995, in *Proceedings of the Third European Symposium on Polar Ozone Research*, *Air Pollut. Res. Rep.*, vol. 56, edited by J. A. Pyle, N. R. P. Harris and G. T. Amanatidis, pp. 484–487, Eur. Comm., Schliersee, Germany, 1995.

Pougatchev, N. S., B. J. Connor, N. B. Jones, and C. P. Rinsland, Infrared measurements of the ozone vertical distribution above Kitt Peak, *J. Geophys. Res.*, *100*(D8), 16,689–16,698, 1995.

Pougatchev, N. S., B. J. Connor, and C. P. Rinsland, Validation of ozone profile retrievals from ground-based solar spectra, *Geophys. Res. Lett.*, *23*(13), 1637–1640, 1996.

Rinsland, C. P., M. A. H. Smith, P. L. Rinsland, A. Goldman, J. W. Brault, and G. M. Stokes, Ground-based infrared spectroscopic measurements of atmospheric hydrogen cyanide, *J. Geophys. Res.*, *87*, 11,119–11,125, 1982.

Rinsland, C. P., R. E. Boughner, J. C. Larsen, G. M. Stokes, and J. W. Brault, Diurnal variations of atmospheric nitric oxide: Ground-based infrared spectroscopic measurements and their interpretation with time-dependent photochemical model calculations, *J. Geophys. Res.*, *89*, 9613–9622, 1984.

Rinsland, C. P., B. J. Connor, N. B. Jones, I. Boyd, W. A. Matthews, A. Goldman, F. J. Murcray, D. G. Murcray, S. J. David, and N. S. Pougatchev, Comparison of infrared and Dobson total ozone columns measured from Lauder, New Zealand, *Geophys. Res. Lett.*, *23*(9), 1025–1028, 1996.

Rinsland, C. P., et al., Northern and southern hemisphere ground-based infrared spectroscopic measurements of tropospheric carbon monoxide and ethane, *J. Geophys. Res.*, *103*(D21), 28,197–28,217, 1998.

Rodgers, C. D., Retrieval of atmospheric temperature and composition from remote measurements of thermal radiation, *Rev. Geophys. Space Phys.*, *14*(4), 609–624, 1976.

Rodgers, C. D., Characterisation and error analysis of profiles retrieved from remote sounding measurements, *J. Geophys. Res.*, *95*(D5), 5587–5595, 1990.

Rodgers, C. D., *Inverse Methods for Atmospheric Sounding: Theory and Practice*, vol. 2, *Series on Atmospheric, Oceanic and Planetary Physics*, World Sci., River Edge, N. J., 2000.

Rothman, L. S., et al., The HITRAN molecular spectroscopic database and HAWKS (HITRAN atmospheric workstation): 1996 edition, *J. Quant. Spectrosc. Radiat. Transfer*, *60*, 665–710, 1998.

Smith, M. A. H., V. Malathy Devi, D. C. Benner, and C. P. Rinsland, Absolute intensities of $^{16}O_3$ lines in the 9–11 μm region, *J. Geophys. Res.*, *106*(D9), 9909–9921, 2001.

Staehelin, J., A. Renaud, J. Bader, R. McPeters, P. Viatte, B. Hoegger, V. Bugnion, M. Giroud, and H. Schill, Total ozone series at Arosa (Switzerland): Homogenization and data comparison, *J. Geophys. Res.*, *103*, 5827–5841, 1998.

Stübi, R., et al., BM-ECC ozone twin flights: Differences between two ozone sonde types, in *Proceedings of the Fifth European Symposium on Stratospheric Ozone*, *Air Pollut. Res. Rep.*, vol. 73, edited by N. R. P. Harris, M. Guirlet, and G. T. Amanatidis, pp. 734–737, Eur. Comm., Saint Jean de Luz, France, 1999.

B. Barret and M. De Mazière, Institut d'Aéronomie Spatiale de Belgique, 3 Av. Circulaire, 1180 Brussels, Belgium. (brice@oma.be)

P. Demoulin, Institut d'Astrophysique et de Géophysique, Université de Liège, 5 Av. de Cointe, 4000 Liège, Belgium.